ROYAL SOCIETY
OF CHEMISTRY

PAPER

Check for updates

3D net-like Co₃O₄@NiO nanostructures for high performance supercapacitors

Xiaochen Sun [ID] and Zengyun Jian*

Co₃O₄@NiO composite electrode materials were successfully synthesized by a two-step hydrothermal method followed by annealing treatment. Due to their three-dimensional network structure, these composite materials exhibited a large specific surface area, enhancing their electrochemical performance. Consequently, the Co₃O₄@NiO electrode demonstrated a specific capacitance of 1306 F g⁻¹ at a current density of 1 A g⁻¹, an excellent specific capacitance retention rate of 95.5% after 3000 cycles even at 8 A g⁻¹ and a coulombic efficiency approaching 100%. These outstanding properties make the Co₃O₄@NiO composite materials promising electrode materials for high performance supercapacitors.

1. Introduction

With the increasing demand for new energy in electronic devices and electric vehicles, the development of energy storage devices has become increasingly important.[1–3] Supercapacitors (SCs) have garnered significant attention as the most promising energy-storage device, which can be attributed to their high power density, fast charging-discharging rate, and cycling stability.[4–12] Based on their working mechanism, SCs can be generally categorized into two categories, including electrical double layer capacitors (EDLCs) and pseudo-capacitors.[13–16] Pseudo-capacitors exhibit fast reversible redox reactions at the near surface of electrode materials, resulting in a higher specific capacitance compared to EDLCs.[17–19] Transition metal oxides, such as ZnO,[20] Co₃O₄,[21] MnO₂,[22] CuO,[23] NiO[24] and V₂O₅,[25] are among the various electrode materials that have been employed in SCs.

Among these materials, Co₃O₄ has been extensively studied due to its high theoretical specific capacitance of 3560 F g⁻¹, environmental friendliness and excellent electrochemical stability.[26] NiO is a promising electrode material for supercapacitors, which has been intensively studied due to its low cost, environmental friendliness, chemical stability and outstanding theoretical specific capacitance (2573 F g⁻¹).[27–32] However, the poor electrical conductivity and low utilization rate of NiO limit its application in the field of high-performance supercapacitors.[33–35]

In order to address these issues, researchers design metal oxide composites by combining two types of metal oxides and harnessing synergistic effects between them to enhance electrochemical performance. Dongqing Su *et al.* reported that ZnO/Co₃O₄ composites exhibited excellent cycle stability as

supercapacitor electrodes, with a specific capacitance of 106.7 F g⁻¹ and a capacitance retention of 102.7 F g⁻¹ after 1000 cycles at 0.5 A g⁻¹.[36] Lei Xing *et al.* prepared Co₃O₄@NiO nanoarrays through a hydrothermal method, achieving a specific capacitance of 608 F g⁻¹ at 2 A g⁻¹.[37] A CuO/NiO/N-rGO composite was fabricated and demonstrated a specific capacitance of approximately 220 F g⁻¹ at a current density of 0.5 A g⁻¹, with the electrode retaining 97% of its specific capacitance after 5000 cycles.[38] Huan Pang *et al.* reported the preparation of a porous ZnO–NiO micropolyhedron material through calcination of the oxalate precursor at 400 °C, which exhibited high specific capacitance (649.0 F g⁻¹ at 5.8 A g⁻¹) and maintained approximately 99.1% of its initial specific capacitance after 400 cycles.[39]

In this work, a three-dimensional mesh composite material was obtained by the hydrothermal reaction. Due to the special structure of the material, more active sites were provided for the reaction process of the material, and the transport path of ions and electrons was shortened. The synergistic effect between the two materials can also improve the electrochemical properties of the electrode materials.

2. Experimental methods

2.1 Fabrication of Co₃O₄

In a typical hydrothermal process, predetermined amounts of Co(NO₃)₂·6H₂O (0.582 g), NH₄F (0.37 g), and CO(NH₂)₂ (0.6 g) were added in 50 ml distilled (DI) water and stirred for half an hour to obtain a homogeneous solution. The precursor solution was then transferred into a 100 ml Teflon-lined stainless steel autoclave with two pieces of Ni foam (1.5 cm × 1.5 cm) immersed in the reaction solution as a substrate. Subsequently, the autoclave was sealed and placed in a reaction tank maintained at 120 °C for 5 h, followed by natural cooling to room temperature. Next, the as-prepared material was washed several

School of Materials and Chemical Engineering, Xi'an Technological University, Xi'an, 710021, China. E-mail: jianzengyun@xatu.edu.cn
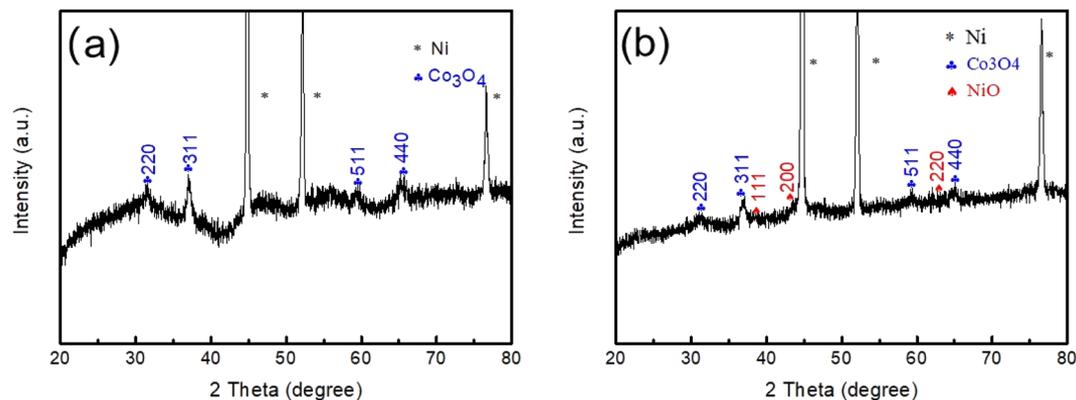
Fig. 1 (a) XRD patterns of Co_3O_4 nanobeams and (b) Co_3O_4@NiO nanostructures.

times with DI water and ethanol to remove any weakly attached materials. The product was then dried at 60 °C for 8 h in a drying oven. Finally, the as-synthesized materials were annealed under an argon atmosphere from room temperature to 450 °C at a heating rate of 5 °C min^{-1} and held at that temperature for another two hours to produce Co_3O_4 nanobeams/Ni foam.

2.2 Fabrication of Co_3O_4@NiO

The hydrothermal method was used, and $Ni(NO_3)_2 \cdot 6H_2O$ (0.582 g), NH_4F (0.14 g), and $CO(NH_2)_2$ (0.6 g) were added in 50 ml DI

water. The mixture was stirred for half an hour to get a homogeneous solution, and the Co_3O_4 nanobeams/Ni foam was placed in the solution and the autoclave was sealed and placed in the reaction tank that was maintained at 105 °C for 5 h, The as-synthesized materials were annealed at 350 °C under an argon atmosphere for 2 h.

2.3 Characterization of the prepared samples

XRD data of the as-synthesized samples were obtained using an X-ray diffractometer (Bruker D2 PHASER) using Cu Kα radiation (λ = 0.1548 nm). The morphology and atomic content were

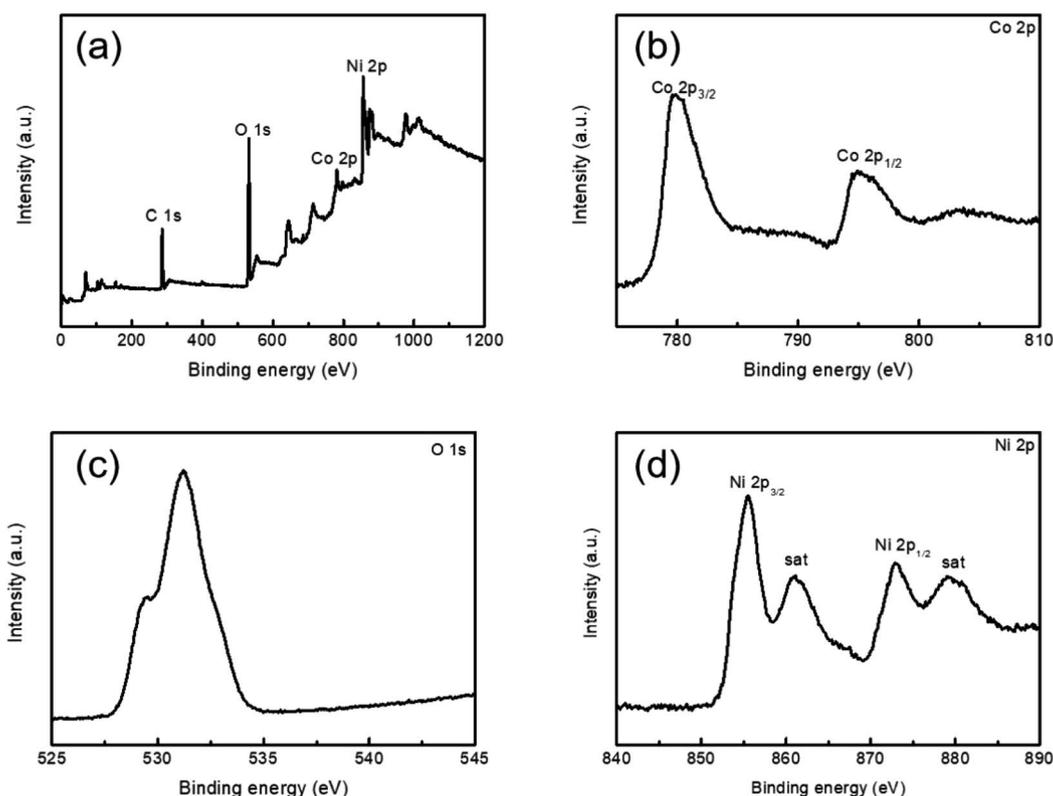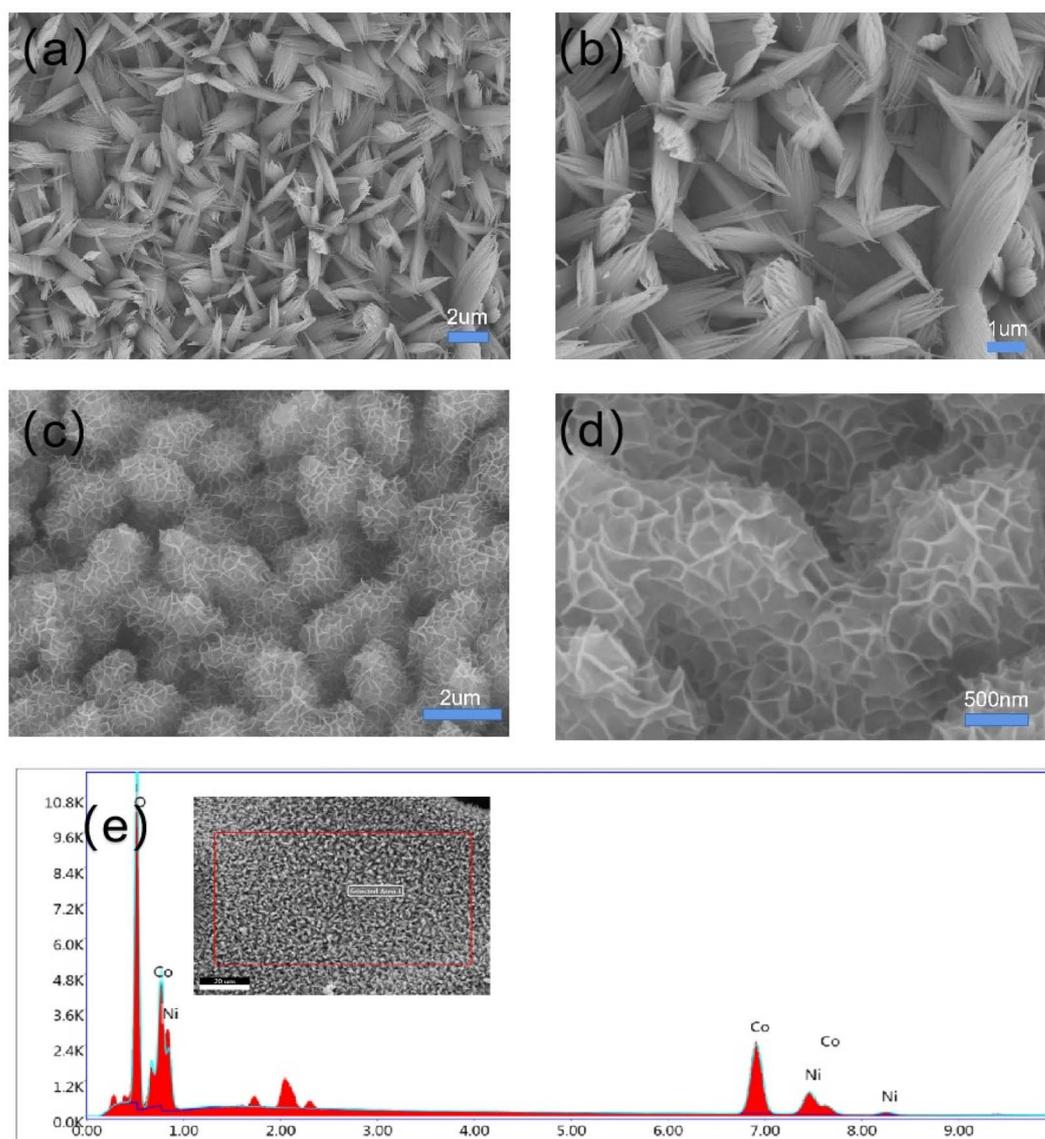**Fig. 2** XPS (a) full survey scan spectrum, (b–d) Co 2p, (c) O 1s, and (d) Ni 2p regions.

Fig. 3 Different magnified SEM images of Co_3O_4 nanobeams (a and b) and Co_3O_4 @NiO 3D net-like nanostructures (c and d), and (e) the corresponding EDS spectra.

Table 1 Composite material element determination

Element	Weight%	Atomic%
O K	21.57	50.30
Co K	56.71	35.90
Ni K	21.72	13.80

characterized by field emission scanning electron microscopy (SEM, ZEISS Sigma 300), high-resolution transmission electron microscopy (HRTEM, FEI Talos F200x) and energy dispersive X-ray spectroscopy (EDX). X-ray photoelectron spectroscopy (XPS) was conducted with a Thermo ESCALAB250 XPS system.

2.4 Electrochemical measurements

All of the electrochemical measurements, including cyclic voltammetry (CV) tests and galvanostatic charge/discharge (GCD) as well as electrochemical impedance spectroscopy (EIS) were carried out in 2 M KOH aqueous solution on a workstation (Princeton 4000A). A three-electrode configuration was adopted in the experiment, in which Hg/HgO and platinum foil were used as reference and counter electrodes, respectively. The typical mass loading of the electrode was about 4 mg. The conditions of EIS tests were as follows: alternating current voltage amplitude 5 mV and a frequency ranging from 0.01 to 1 $\times 10^5$ Hz at open circuit potential.
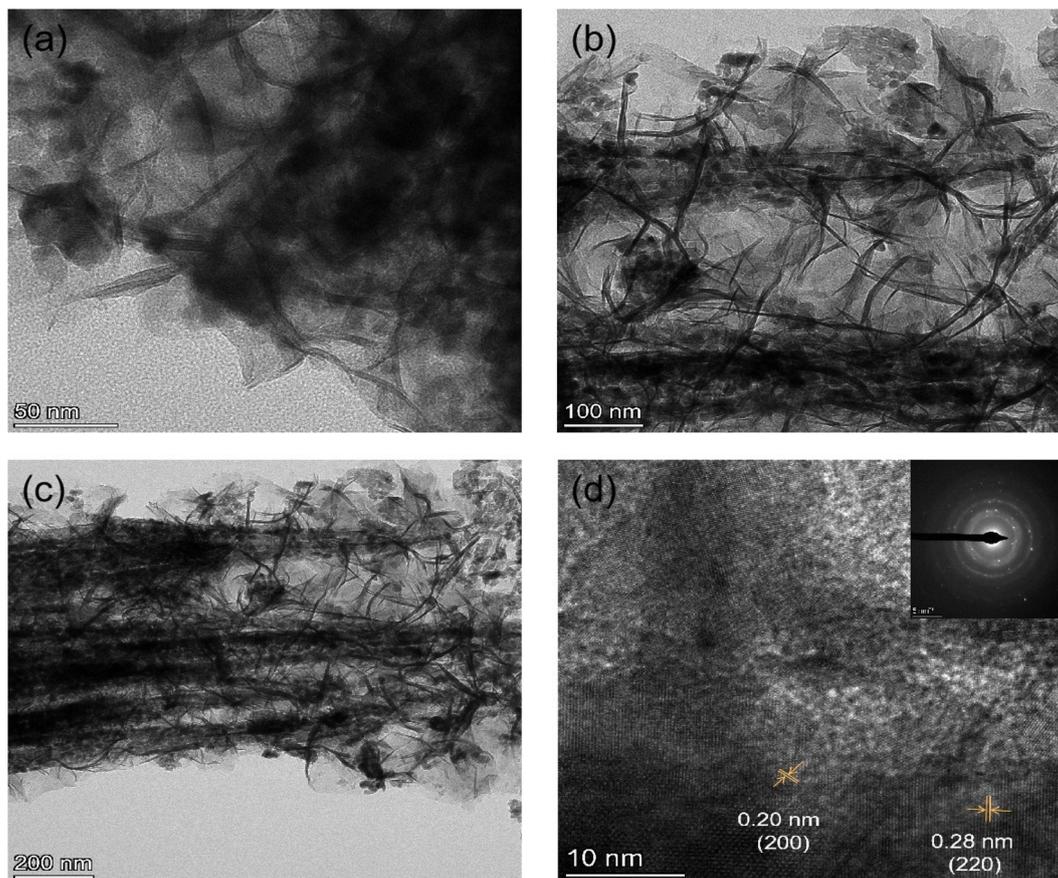
Fig. 4 (a–c) TEM images and (d) corresponding HRTEM images of the Co_3O_4@NiO electrode material.

3. Results and discussion

In order to investigate the phase and crystal structures of the synthesized samples, XRD technology was employed and the observed results are presented in Fig. 1a and b. As depicted in Fig. 1a, the XRD pattern of Co_3O_4 on Ni foam exhibited several distinct diffraction peaks. The identified diffraction peaks at $44.7°$, $52.1°$ and $76.6°$ corresponded to the nickel foam substrate. Additionally, several other diffraction peaks appearing at $31.3°$, $36.9°$, $59.3°$ and $65.2°$ were assigned to the (220), (311), (511) and (440) planes of the cubic Co_3O_4 phase (JCPDS card no. 42-1467), respectively. In addition, diffraction peaks assigned without NiO or Co_3O_4 were detected, indicating the high purity of Co_3O_4. Fig. 1b shows the XRD pattern of the Co_3O_4@NiO nanonet. It could be seen that the diffraction peaks located at $37.2°$, $43.3°$ and $62.9°$ were also seen which corresponded to the NiO crystal planes of (111), (200) and (220), respectively. These peaks were well-matched with the cubic NiO phase (JCPDS card no. 47-1049). No other miscellaneous characteristic peaks were detected in the xrd pattern, indicating that the prepared Co_3O_4@NiO samples have high purity. The strong diffraction peaks of the Co_3O_4@NiO composite clearly confirmed the well-crystallinity of the synthesized product.

To further analyze the chemical bonding state of the electrode materials. XPS measurements were conducted. Fig. 2a displays a full survey scan spectrum, which indicated the existence of Ni, Co, O and C elements. Fig. 2b shows the Co 2p XPS spectrum, with two distinct peaks located in the binding energies of 780.1 and 795.3 eV, corresponding to Co $2p_{3/2}$ and Co $2p_{1/2}$, consistent with the presence of Co_3O_4. Fig. 2c demonstrates the O 1s spectrum; there were two peaks at 529.1 and 531.1 eV; the low binding energy at 529.1 eV is due to the OH^- species absorbed on the surface, and the high binding energy at 531.1 eV was the defect sites with low oxygen coordination. Fig. 2d exhibits the Ni 2p spectrum; there were two binding energy peaks at 529.1 and 531.1 eV, which corresponded to Ni $2p_{3/2}$ and Ni $2p_{1/2}$ levels, respectively. Two satellite peaks (sat.) were at 861.1 and 879.4 eV.

The general morphologies of Co_3O_4 nanobeams and Co_3O_4@NiO 3D net-like nanostructures were verified by SEM. Fig. 3a and b show the SEM images of Co_3O_4 nanobeams on the Ni foam. It was revealed that Co_3O_4 nanobeams were coated on the surface of the Ni foam with a length of several micrometres. As described in Fig. 3c and d, the SEM images of the Co_3O_4@NiO composites on the Ni foam at different magnifications indicated that densely assembled NiO nanosheets were anchored onto the entire Co_3O_4 nanobeam surface, forming three-dimensional interconnection network structures. The full lengths of the Co_3O_4@NiO nanonet were several micrometres. Such three-dimensional interconnection network structures

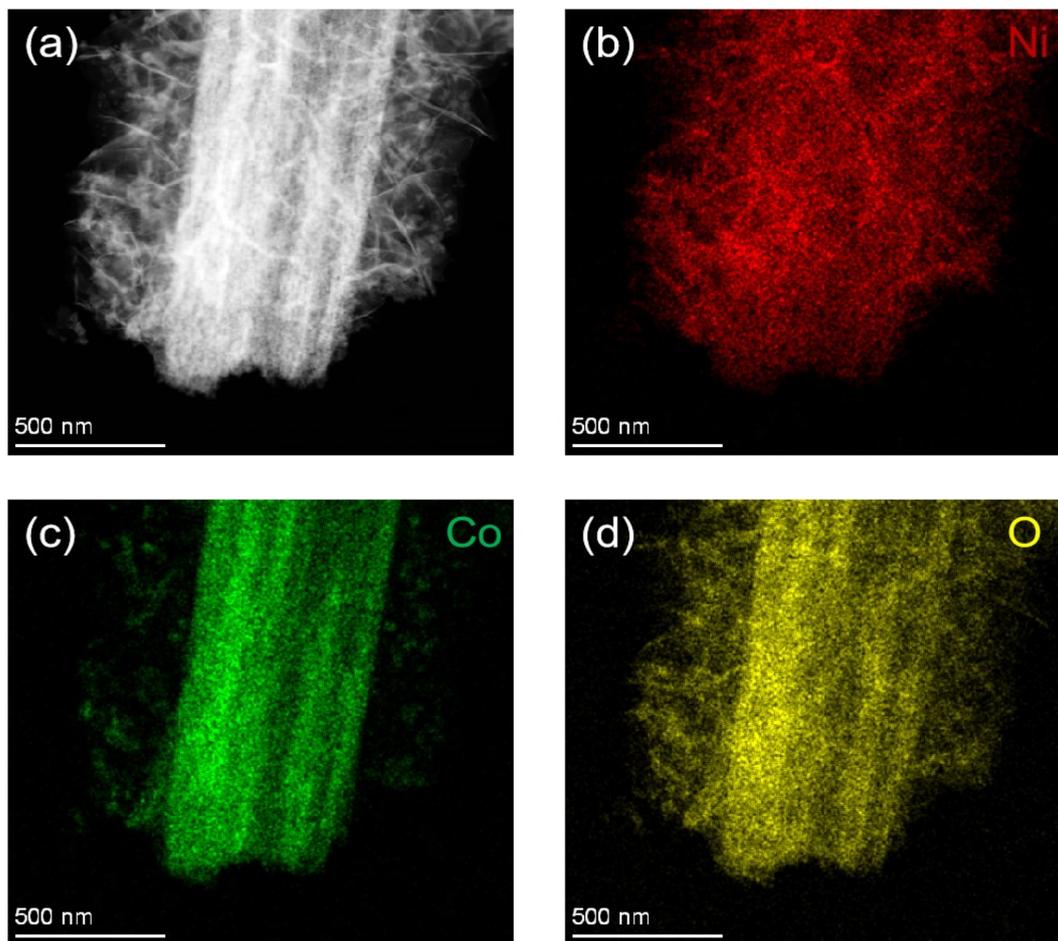**Fig. 5** (a–d) EDS mapping images of 3D net-like Co_3O_4@NiO nanostructures grown on Ni foam.

could effectively increase specific surface area of the composite and provide more active sites during redox reactions and thus greatly enhance the specific capacitance and rate capability. The EDS diagram shows the distribution of the elements of the material in Fig. 3e. From Table 1, we could see that the contents of O and Co elements were relatively rich with a ratio close to that of Co_3O_4. At the same time, the atomic ratios of Ni and O were close to that of NiO.

The TEM tests were carried out to further investigate the morphology structure of the Co_3O_4@NiO 3D net-like nanostructures. Fig. 4a–c demonstrate the TEM images of Co_3O_4@NiO composites at different magnifications, as it could be seen that the NiO nanosheets with a thickness of about 40–60 nm were uniformly covered on the Co_3O_4 nanobeam surface, forming complex structures. The net-like structure will also greatly increase the electrode–electrolyte contact area and thus further enhanced the electrochemical performance. From the HRTEM image of Co_3O_4@NiO in Fig. 4d, it could be seen that the lattice spacings were measured to be 0.28 and 0.20 nm, in agreement with the interplanar spacing of Co_3O_4 (220) and NiO (200) planes, which indicated that the resultant products contained Co_3O_4@NiO materials. The inset of Fig. 4d presents

a SAED pattern, suggesting that the samples possess polycrystalline characteristics.

The elemental mapping images of the Co_3O_4@NiO composites are shown in Fig. 5a–d. It was clear that the Ni, Co, and O elements were uniformly dispersed in three-dimensional porous network structures.

In order to further study the electrochemical performance of Co_3O_4, and Co_3O_4@NiO, cyclic voltammetry (CV) and galvanostatic charge–discharge were conducted. Fig. 6a illustrates the CV plots of Co_3O_4 and Co_3O_4@NiO nanonet at a scan rate of 10 mV s^{-1} within the potential range of 0–0.7 V. It was evident that the integrated area under the CV curves of Co_3O_4@NiO is larger than that of Co_3O_4, indicating that the hybrid composite possesses a higher specific capacitance compared to an individual material.

As shown in Fig. 6b, the CV curves of Co_3O_4 and Co_3O_4@NiO at different scan rates ranging from 5–70 mV s^{-1} demonstrated excellent reversibility for this asymmetric supercapacitor. Moreover, these CV curves exhibited a couple of redox peaks primarily governed by reversible redox reactions involving Ni^{2+}/Ni^{3+} and Co^{2+}/Co^{3+}. The main faradaic redox reaction could be expressed as follows:
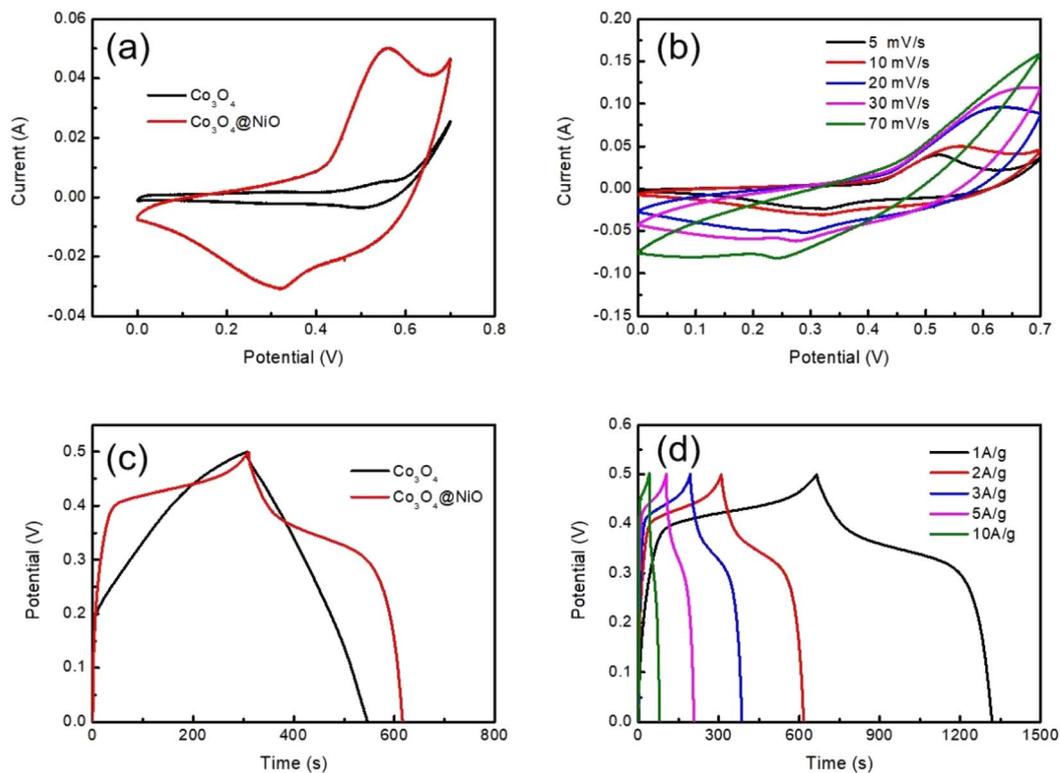
Fig. 6 (a) A comparison of CV curves of Co_3O_4 and $Co_3O_4@NiO$ products at a scan rate of 10 mV s^{-1} (b) CV curves of $Co_3O_4@NiO$ at different scan rates (c) GCD curves of Co_3O_4 and $Co_3O_4@NiO$ products at 2 A g^{-1} current density (d) GCD curves of the $Co_3O_4@NiO$ composite material at different current densities.
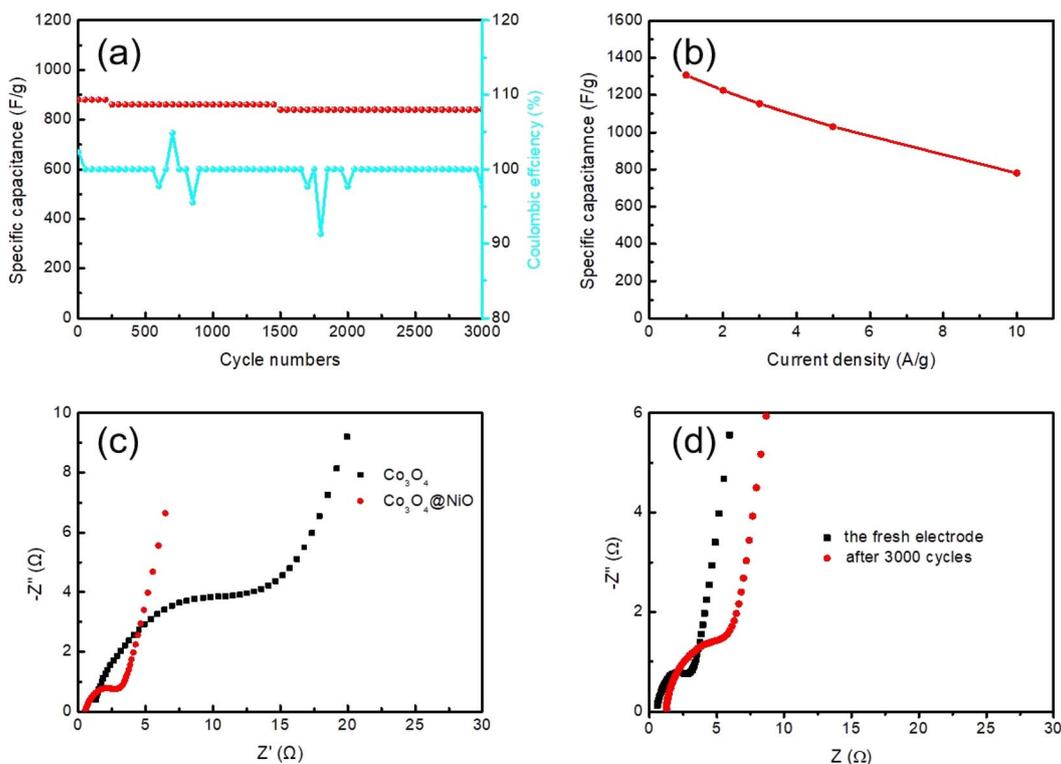
Fig. 7 (a) Cycling performance and coulombic efficiency of $Co_3O_4@NiO$ products, (b) specific capacitance of $Co_3O_4@NiO$ products at different current densities. (c) Nyquist plots of Co_3O_4 nanobeams and $Co_3O_4@NiO$ 3D net-like nanostructures and (d) Nyquist plots of the fresh electrode and after 3000 cycles.

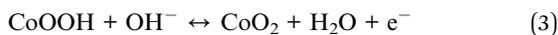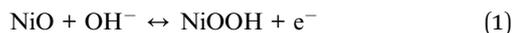$$NiO + OH^- \leftrightarrow NiOOH + e^- \qquad (1)$$

$$Co_3O_4 + OH^- + H_2O \leftrightarrow 3CoOOH + e^- \qquad (2)$$

$$CoOOH + OH^- \leftrightarrow CoO_2 + H_2O + e^- \qquad (3)$$

Fig. 6c presents the GCD curves of Co_3O_4@NiO and Co_3O_4 nanobeams at a current density of 2 A g^{-1}. Remarkably, it can be observed that the discharge time for the Co_3O_4@NiO electrode is longer than that for the pure Co_3O_4 electrode, implying that the specific capacitances are greatly improved after the recombination of NiO because of the synergistic effect between Co_3O_4 and NiO. Fig. 6d shows GCD curves of the Co_3O_4@NiO composite electrode at different current densities from 1 to 10 A g^{-1}. The discharge time is 653, 306, 1192, 103 and 40 s, respectively.

Fig. 7a demonstrates the excellent cycling performance and coulombic efficiency of the supercapacitor with a remarkable capacitance retention of 95.5% at a constant current density of 8 A g^{-1} for 3000 cycles, indicating its remarkable cycling stability. The coulombic efficiency of the supercapacitor electrodes was close to 100%. Fig. 7b exhibits specific capacitance of Co_3O_4@NiO at different current densities; the Co_3O_4@NiO delivered a high specific capacitance of 1306, 1224, 1152, 1030, and 780 F g^{-1} at 1, 2, 3, 5 and 10 A g^{-1}, respectively. As shown in Fig. 7c, electrochemical impedance spectra (EIS) measurement was carried out, which demonstrated the ion diffusion and charge transfer process. All samples exhibited a small diameter semicircle in the high frequency area, which represented the charge transfer resistance (R_{ct}). It could be seen that composite materials had a lower charge transfer resistance. Nyquist plots of the Co_3O_4@NiO electrode before and after cycles are shown in Fig. 7d, indicating that R_{ct} increases and the slope of the straight line tends to reduce simultaneously.

4. Conclusions

In summary, we have successfully fabricated Co_3O_4@NiO composite electrode materials on Ni foam by a hydrothermal process and annealing treatment, yielding a supercapacitor electrode material. The unique structure of these electrode materials, which enhances the specific surface area and provides additional active sites during the chemical reaction process, concurrently offers more transmission paths for ion and electron transport. The integrated electrode demonstrates exceptional electrochemical performance, characterized by high specific capacitance, low resistance and superior cycling stability. This promising electrode material is ideal for next generation energy storage devices.

Conflicts of interest

There are no conflicts to declare.

Acknowledgements

References

1 C. Liu, F. Li, L. P. Ma and H. M. Cheng, *Adv. Mater.*, 2010, **22**, E28–E62.

2 J. Tian, Z. Xing, Q. Chu, Q. Liu, A. M. Asiri, A. O. Al-Youbi and X. Sun, *CrystEngComm*, 2013, **15**, 8300–8305.

3 P. Simon and Y. Gogotsi, *Nat. Mater.*, 2008, **7**, 845–854.

4 Z. Yang, Z. Li, P. Li, C. Gao and H. Zhang, *J. Mater. Sci.*, 2020, **55**, 1659–1672.

5 Y. F. Ren, Z. L. He, H. Z. Zhao and T. Zhu, *Rare Met.*, 2022, **41**, 830–835.

6 F. F. Zhu, L. Sun, Y. Liu and W. D. Shi, *J. Mater. Chem. A*, 2022, **10**, 21021–21030.

7 T. Zhu, J. Pan, Z. Y. An, R. J. Zhe, Q. H. Ou and H.-E. Wang, *J. Mater. Chem. A*, 2022, **10**, 20375–20385.

8 F. Ren, T. Zhu, Y. D. Liu, Q. B. Liu and Q. Y. Yan, *Small*, 2021, **17**, 2008047.

9 Y. Wang and Y. Xia, *Adv. Mater.*, 2013, **25**, 5336–5342.

10 G. Wang, L. Zhang and J. Zhang, *Chem. Soc. Rev.*, 2012, **41**, 797–828.

11 B. Pal, S. Yang, S. Ramesh, V. Thangadurai and R. Jose, *Nanoscale*, 2019, **1**, 3807–3835.

12 R. S. Devan, R. A. Patil, J. H. Lin and Y. R. Ma, *Adv. Funct. Mater.*, 2012, **22**, 3326–3370.

13 W. Zhou, X. Cao, Z. Zeng, W. Shi, Y. Zhu, Q. Yan, H. Liu, J. Wang and H. Zhang, *Energy Environ. Sci.*, 2013, **6**, 2216–2221.

14 Y. Shao, M. F. El-Kady, J. Sun, Y. Li, Q. Zhang, M. Zhu, H. Wang, B. Dunn and R. B. Kaner, *Chem. Rev.*, 2018, **118**, p9233.

15 Z. Y. Yin, J. X. Zhu, Q. Y. He, X. H. Cao, C. L. Tan, H. Y. Chen, Q. Y. Yan and H. Zhang, Graphene-Based Materials for Solar Cell Applications, *Adv. Energy Mater.*, 2014, **4**, 1300574.

16 C. An, Y. Zhang, H. Guo and Y. Wang, *Nanoscale*, 2019, 4644–4658.

17 P. Yang, X. Xiao, Y. Li, Y. Ding, P. Qiang, X. Tan, W. Mai, Z. Lin, W. Wu, T. Li, H. Jin, P. Liu, J. Zhou, C.-P. Wong and Z.-L. Wang, *ACS Nano*, 2013, **7**, 2617–2626.

18 T. Brousse, D. Belanger and J. W. Long, To be or Not to be Pseudocapacitive, *J. Electrochem. Soc.*, 2015, **162**, A5185.

19 H. Tong, S. H. Yue, L. Lu, F. Q. Jin, Q. W. Han, X. G. Zhang and J. Liu, *Nanoscale*, 2017, **9**, 16826–16835.

20 N. Hu, W. H. Gong, L. Huang and P. K. Shen, *J. Mater. Chem. A*, 2019, 1273–1280.

21 Y. Lu, B. Deng, Y. Liu, J. Wang and G. Xu, Nanostructured Co3O4 for achieving high-performance supercapacitor, *Mater. Lett.*, 2021, **285**, 129101.

22 Y. Zhang, M. Huang, F. Li, X.-L. Wang and Z. Wen, *J. Power Sources*, 2014, **246**, 449–456.

23 S. Chatterjee, A. Ray, M. Mandal, S. Das and S. K. Bhattacharya, *J. Mater. Eng. Perform.*, 2020, **29**, 8036–8048.

24 M. Huang, F. Li, J. Ji, Y. Zhang, X. Zhao and X. Gao, *CrystEngComm*, 2014, **16**, 2878–2884.

25 Q. Qu, L. Liu, Y. Wu and R. Holze, *Electrochim. Acta*, 2013, **96**, 8–12.

26 R. S. Kate, S. A. Khalate and R. J. Deokate, *J. Alloys Compd.*, 2018, **734**, 89–111.

27 Z. Xiao, L. Fan and B. Xu, *ACS Appl. Mater. Interfaces*, 2017, **9**, 41827–41836.

28 X. Ren, C. Guo, L. Xu, T. Li, L. Hou and Y. Wei, *ACS Appl. Mater. Interfaces*, 2015, **7**, 19930–19940.

29 S. Ramesh, K. Karuppasamy, S. Msolli, H. S. Kim, H. S. Kim and J. H. Kim, *New J. Chem.*, 2017, **41**, 15517–15527.

30 W. Huang, L. Li, D. Liang, W. Zhou, H. Wang, Z. Lu, S. Yu and Y. Fan, *Inorg. Chem. Front.*, 2019, **6**, 2927–2934.

31 X. Q. Tian, C. M. Cheng, L. Qian, B. Z. Zheng, H. Y. Yuan, S. P. Xie, D. Xiao and M. M. F. Choi, *J. Mater. Chem.*, 2012, **22**, 8029–8035.

32 S. Vijayakumar, S. Nagamuthu and G. Muralidharan, *ACS Appl. Mater.*, 2013, **5**, 2188–2196.

33 X. Long, Z. Zeng, E. Guo, X. Shi, H. Zhou and X. Wang, *J. Power Sources*, 2016, **325**, 264–272.

34 C. Z. Wei, H. Pang, C. Cheng, J. H. Zhao, P. W. Li and Y. K. Zhang, *CrystEngComm*, 2014, **16**, 4169.

35 C. M. Zhou, X. M. Cao, Z. J. Sun, Y. Wei and Q. G. Zhang, *ChemElectroChem*, 2022, **9**, e202101675.

36 D. Q. Su, L. M. Zhang, Z. H. Tang, T. T. Yu, H. L. Liu, J. H. Zhang, Y. J. Liu, A. H. Yuan and Q. H. Kong, *J. Nanosci. Nanotechnol.*, 2018, **18**, 4884–4890.

37 L. Xing, Y. Dong, F. Hu, X. Wu and A. Umar, *Dalton Trans.*, 2018, **47**, 5687–5694.

38 V. Kakani, S. Ramesh, H. M. Yadav, K. A. Kumar, S. Shinde, S. Sandhu, L. N. D. Quang, H. S. Kim, H. Kim and C. Bathula, Facile synthesis of CuO/NiO/nitrogen doped rGO by ultrasonication for high performance supercapacitors, *J. Alloys Compd.*, 2020, **847**, 156411.

39 H. Pang, Y. H. Ma, G. C. Li, J. Chen, J. S. Zhang, H. H. Zheng and W. Dua, *Dalton Trans.*, 2012, **41**, 13284–13291.